Volume 12 | Number 33 | 7 September 2016 | Pages 6885–7064

Soft Matter

www.softmatter.org

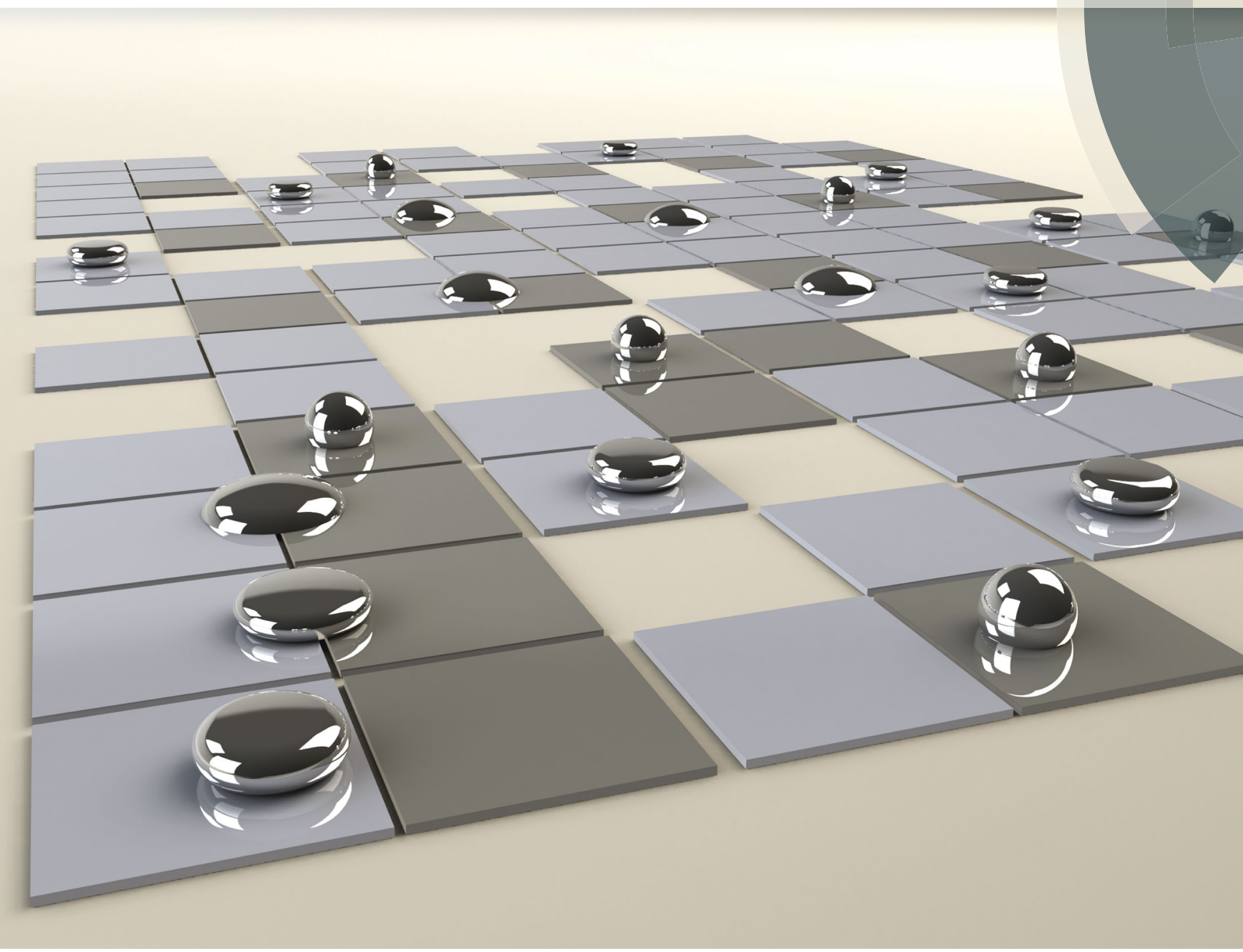

ISSN 1744-683X

ROYAL SOCIETY OF CHEMISTRY

PAPER

Eui-Hyeok Yang *et al.*

Lateral actuation of an organic droplet on conjugated polymer electrodes *via* imbalanced interfacial tensions

175 YEARS

Soft Matter

PAPER

Cite this: *Soft Matter*, 2016, **12**, 6902

Lateral actuation of an organic droplet on conjugated polymer electrodes *via* imbalanced interfacial tensions†

Wei Xu, Jian Xu, Xin Li, Ye Tian, Chang-Hwan Choi and Eui-Hyeok Yang*

Received 26th May 2016,
Accepted 8th July 2016

DOI: 10.1039/c6sm01223j

www.rsc.org/softmatter

This paper presents a new mechanism for the controlled lateral actuation of organic droplets on dodecylbenzenesulfonate-doped polypyrrole (PPy(DBS)) electrodes at low voltages (~0.9 V) in an aqueous environment. The droplet actuation is based on the tunable surface wetting properties of the polymer electrodes induced by electrochemical redox reactions. The contact angle of a dichloromethane (DCM) droplet on the PPy(DBS) surface switches between ~119° upon oxidation (0.6 V) and ~150° upon reduction (−0.9 V) in 0.1 M $NaNO_3$ solution. The droplet placed across the reduced and oxidized PPy(DBS) electrodes experiences imbalanced interfacial tensions, which prompt the actuation of the droplet from the reduced electrode to the oxidized electrode. The lateral actuation of DCM droplets on two PPy(DBS) electrodes is demonstrated, and the actuation process is studied. The driving force due to the imbalanced interfacial tensions is estimated to be approximately 10^{-7} N for a 6 μL droplet.

1. Introduction

Conjugated polymers, such as dodecylbenzenesulfonate-doped polyaniline (PANI(DBS)), perfluorooctanesulfonate-doped polypyrrole (PPy(FPOS)), and dodecylbenzenesulfonate-doped polypyrrole (PPy(DBS)), exhibit tunable surface wetting properties upon the application of electrical stimuli, which have been used for the manipulation of droplets at low voltages (1–5 V).[1–5] Isaksson *et al.* demonstrated the spreading of a water droplet on a PANI film with a wettability gradient generated by a biased electrical field (5 V) near the film.[6] While Chang *et al.* has demonstrated the actuation of a water droplet on the microstructured PPy(FPOS) grown on a mesh substrate,[5] the intrinsic toxicity of the FPOS limits its applicability.[7] Among the conductive polymers, polypyrrole (PPy) shows high electrical conductivity and good environmental stability and has been one of the most widely used polymers.[3] Causely *et al.* demonstrated an electrochemically-induced fluid movement in a PPy(DBS)-coated channel by applying a reduction potential at one end of the channel.[8] Chatzipirpiridis *et al.* demonstrated a three-dimensional robotic system for the pickup, transport, and release of drops using polypyrrole architectures.[9] Tsai[10] and Xu[11] demonstrated the unidirectional transportation of both aqueous and organic droplets on tilted PPy(DBS) surfaces, where the droplet behavior was largely affected by the tilting angle of the substrate. In addition to aqueous droplets, water-immiscible organic reagents (*e.g.* dichloromethane (DCM)) are of significance in various applications, such as drug delivery and miniaturized droplet reaction systems;[12–14] yet the controlled actuation of organic droplets in aqueous environment has been less explored.

Here, we show a low-voltage (−0.9 V) controlled lateral actuation of an organic liquid droplet (DCM), in an aqueous environment on PPy(DBS) electrodes, and elucidate the mechanism of droplet actuation. We demonstrate that the droplet is driven by a net force induced by the difference in lateral interfacial tensions generated between the adjacent PPy(DBS) electrodes under reduction and oxidation, respectively. We systematically exploit the behaviors of the droplet during the actuation process, including the displacement, velocity, contact angles, and forces.

2. Actuation mechanism

Fig. 1 illustrates the actuation mechanism of an organic droplet on PPy(DBS) electrodes in an aqueous electrolyte (0.1 M $NaNO_3$) environment. The PPy(DBS) electrodes are initially in an oxidized state by applying a voltage of 0.6 V (*vs.* counter electrode). Next, an organic droplet (*e.g.*, DCM) is placed on top of two PPy(DBS) electrodes so that it partially covers both electrodes. Once a reductive voltage of −0.9 V (*vs.* counter electrode) is applied to one of the two PPy(DBS) electrodes (*e.g.*, the left in Fig. 1), the PPy(DBS) surface exposed to the electrolyte is reduced along with

Department of Mechanical Engineering, Stevens Institute of Technology, New Jersey, 07030, USA. E-mail: Eui-Hyeok.Yang@stevens.edu

† Electronic supplementary information (ESI) available: Schematic of experimental setup and the calculation of the interfacial tension of a flattened sessile droplet. See DOI: 10.1039/c6sm01223j

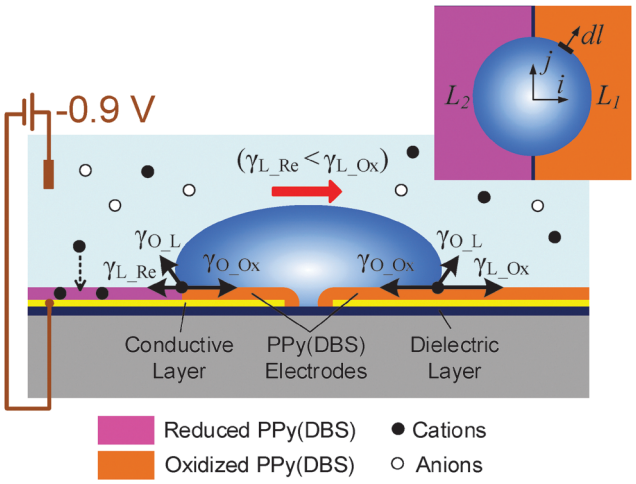

Fig. 1 Scheme illustrating the actuation mechanism of an organic droplet on the PPy(DBS) electrodes in an aqueous electrolyte, driven by imbalanced lateral interfacial tensions upon the application of a low voltage. The application of a reductive voltage on the PPy(DBS) electrode (left) reduces the area exposed to the electrolyte, resulting in imbalanced lateral interfacial tensions (*i.e.*, $\gamma_{L\_Re} < \gamma_{L\_Ox}$) on the organic droplet aligned between two PPy(DBS) electrodes. As a result, the droplet moves from the activated PPy(DBS) electrode (left) to the non-activated PPy(DBS) electrode (right) at low voltages.

the absorption of cations from the electrolyte into PPy(DBS) for charge neutralization.[4] However, the electrode area underneath the droplet on the activated PPy(DBS) electrode still remains oxidized since the droplet acts as a barrier against the absorption of cations into the PPy(DBS) film to accomplish the reduction of PPy(DBS).[4,15–17] The PPy(DBS) on the non-activated electrode is also in an oxidized state. Here, the lateral interfacial tensions experienced by the droplet along the droplet boundary are now in an imbalanced state, since a reduced PPy(DBS) surface is more hydrophilic than an oxidized PPy(DBS) surface.[3,4,10] As a result, a lateral driving force is generated on the droplet as

$$F_x = \int_{L_1} (\gamma_{L\_Ox} - \gamma_{O\_Ox})_1 (\vec{i} \cdot d\vec{l}) - \int_{L_2} (\gamma_{L\_Re} - \gamma_{O\_Ox})_2 (\vec{i} \cdot d\vec{l}), \quad (1)$$

where γ_{L_Ox}, γ_{O_Ox}, and γ_{L_Re} are the interfacial tensions of the aqueous electrolyte-oxidized PPy(DBS) interface, the organic droplet-oxidized PPy(DBS) interface, and the aqueous electrolyte-reduced PPy(DBS) interface, respectively, and L_1 and L_2 are the contact lines of the droplet on non-activated (oxidized) and activated (reduced) electrodes, respectively.[18] Since the γ_{L_Re} is smaller than the γ_{L_Ox} (the reduced PPy(DBS) surface is more hydrophilic), the driving force is directed from the activated (reduced) PPy(DBS) electrode to the non-activated (oxidized) PPy(DBS) electrode (*i.e.*, from the left to the right as shown in Fig. 1) according to eqn (1). If the driving force due to the imbalanced lateral interfacial tensions is larger than the resistance forces, it results in a lateral motion of the droplet to the non-activated PPy(DBS) electrode.

3. Results and discussion

3.1. Tunable wetting of PPy(DBS) surfaces

We analyzed the tunable wettability of PPy(DBS) surfaces during the oxidation and reduction processes by means of measurement of the change in the apparent contact angles of DCM droplets on PPy(DBS) surfaces immersed in 0.1 M $NaNO_3$ solution. As shown in Fig. 2a, the contact angles of the DCM droplets showed a clear change upon the oxidation and reduction of PPy(DBS) surfaces. The contact angles on oxidized surfaces significantly increased to $\sim 150^\circ$ upon reduction and showed an almost constant value even after multiple redox cycles. The contact angles of the droplets upon oxidation gradually increased over multiple redox cycles, starting from $\sim 70^\circ$ in the beginning and then becoming stable at $\sim 119^\circ$ after around ten cycles (*i.e.*, in the stabilized state). The change of the wetting properties of the surface before reaching the stabilized state was related to the change in surface roughness, the influx of water from the electrolyte into the polymer, or the accumulation of surfactant dopants on the polymer surface.[3,19–21] In the stabilized state, the difference in the contact angles of the DCM droplets on oxidized and reduced PPy(DBS) surfaces was approximately 31°, indicating the tunable wettability of PPy(DBS) surfaces during the redox cycles. Fig. 2b shows the typical profile of the droplet during the redox cycles on the PPy(DBS) surface in the stabilized state: the contact angle was $\sim 119^\circ$ on an oxidized surface (Fig. 2b-i), and was increased to $\sim 150^\circ$ upon reduction, along with the flattening of the droplet (Fig. 2b-ii). New DCM droplets were used in each redox cycle for contact angle measurements in Fig. 2a. When a single droplet was used during multiple redox cycles, it showed a similar change in the contact angle and droplet shape.[4]

The change in the contact angle is due to two contributing factors. First, the surfactant dopant molecules (DBS^-) reorient in PPy(DBS) during the reduction, exposing the hydrophilic (or oleophobic) sulfonic acid groups at the outermost surface (Fig. 2b-iv).[3,22] Therefore, the reduced polymer surface demonstrates a stronger affinity for water (*i.e.*, more hydrophilic or oleophobic) than the organic liquid, which reduces the interfacial tension at the aqueous electrolyte–PPy(DBS) interface (*i.e.*, γ_{L_Ox} becomes γ_{L_Re}). As a consequence of the decreased interfacial tension at the electrolyte–PPy(DBS) interface (*i.e.*, γ_{L_Re}), the contact angle of the droplet increases according to the Young's equation as:

$$\gamma_{L\_O} \cos\theta = \gamma_{L\_Re} - \gamma_{O\_Ox}, \quad (2)$$

where γ_{L_O} is the interfacial tension at the electrolyte–droplet interface, and θ is the apparent contact angle of a droplet. Second, although the majority of the DBS^- molecules are locked in the PPy(DBS) matrix due to the bulkiness of volume,[23–25] a minute amount of DBS^- molecules desorbs from the PPy(DBS) surface and is released into the surrounding electrolyte during the reduction.[11] The released DBS^- molecules accumulate at the interface between the organic droplet and the aqueous electrolyte (Fig. 2b-iv), resulting in a decrease in the interfacial tension at the electrolyte–droplet interface (γ_{L_O}) during the reduction. The release of surfactants from PPy(DBS) surfaces and the consequent effect on the change of interfacial tension have been

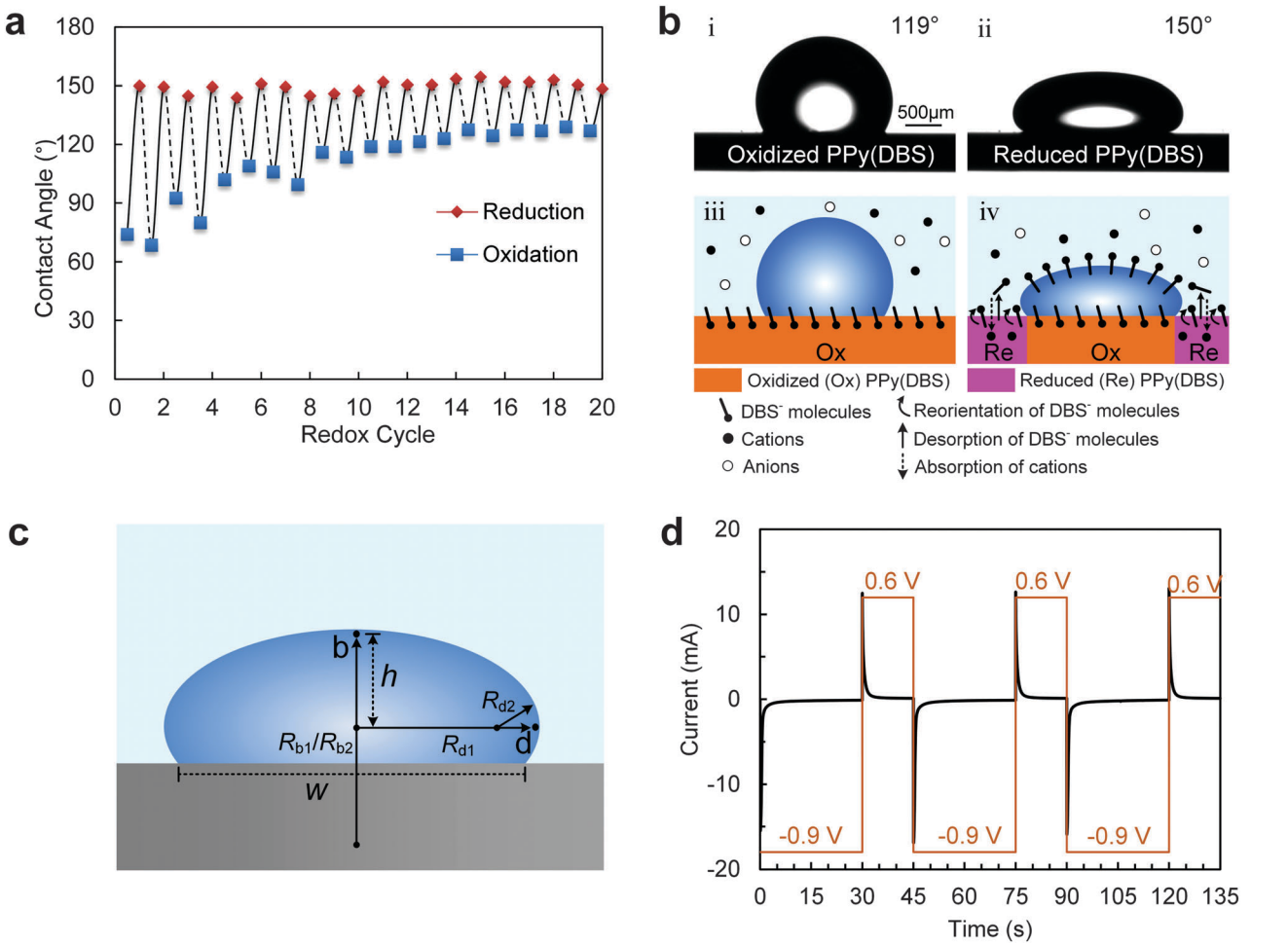

Fig. 2 (a) Change in the contact angle of DCM droplets on a PPy(DBS) surface during multiple redox cycles. (b) (i) Apparent contact angle of a DCM droplet on an oxidized PPy(DBS) surface in 0.1 M $NaNO_3$ solution; (ii) flattening and contact angle increase of a DCM droplet when a reduction voltage of −0.9 V was applied; (iii)–(iv) schematics illustrating the change of the contact angle of a DCM droplet on a PPy(DBS) surface during redox. (c) Schematic of the cross-section view of a flattened sessile droplet on a substrate. R_{d1} and R_{d2} are the principal radii of curvature at the position where the radius of the flattened droplet is maximum (*i.e.*, position d), and R_{b1} and R_{b2} are the principal radii of curvature at the vertex of the droplet (*i.e.*, position b). h is the distance between the vertex of the flattened droplet and the horizontal plane where the radius of the droplet is maximum. W is the width of the droplet. (d) Chronoamperometric current curve of the oxidation (0.6 V) and reduction (−0.9 V) processes of a PPy(DBS) film.

particularly studied in our previous work.[11] The interfacial tension at the electrolyte–droplet interface (γ_{L_O}) was measured using a pendant droplet method before the reduction, which is based on the Young–Laplace equation.[26,27] The interfacial tension of the flattened droplet on the reduced PPy(DBS) surface (as shown in Fig. 2b-ii) was estimated based on the balance between the Laplace pressure and the hydrostatic pressure of the droplet, which is represented as:

$$\gamma_{L\_O} = \frac{\Delta\rho g h}{\left(\frac{1}{R_{d1}} + \frac{1}{R_{d2}} - \frac{1}{R_{b1}} - \frac{1}{R_{b2}}\right)}, \quad (3)$$

where $\Delta\rho$ is the difference in density between the droplet (*e.g.*, DCM) and surrounding medium (*e.g.*, 0.1 M $NaNO_3$), g is the constant acceleration due to gravity, h is the distance between the vertex of the flattened droplet and the horizontal plane where the radius of the droplet is maximal, R_{d1} and R_{d2} are the principal radii of curvature at the position where the radius of the flattened droplet is maximal (*i.e.*, position d in Fig. 2c), and R_{b1} and R_{b2} are the principal radii of curvature at the vertex of the droplet (*i.e.*, position b in Fig. 2c). The derivation process is shown in the ESI.† For the droplet shown in Fig. 2b, the interfacial tension at the electrolyte–droplet interface (γ_{L_O}) was calculated to significantly decrease from 27.8 mN m^{-1} to 0.27 mN m^{-1}. The decrease of the interfacial tension further amplifies the change in the contact angle when it is larger than 90°, according to eqn (2).

The decrease of the interfacial tension at the electrolyte–droplet interface (γ_{L_O}) also results in the shape change (*i.e.*, flattening) of the droplet from a spherical cap shape to an ellipsoid (Fig. 2b-ii), due to the greater influence of the gravitational force than the interfacial tension force on the droplet shape. The greater influence of the gravitational force is indicated by the increase of bond number (Bo). The number

Bo is the ratio of the gravitational and surface tension forces, defined by

$$\mathrm{Bo} = \frac{\Delta\rho g R^2}{\gamma_{\mathrm{L\_O}}}, \quad (4)$$

where R is the characteristic length (*e.g.*, the radius of the droplet).[18] The number Bo of the droplet as shown in Fig. 2b increases from 0.1 to 10.4 after the reduction with a decrease of the interfacial tension. A higher Bo number indicates the increased effect of gravitational force on the droplet shape, causing the flattening of the droplet.[11] In addition, the retentive force of the organic droplet on the PPy(DBS) surface, attributed to solid–liquid interaction,[28,29] is decreased with the decrease of the electrolyte–droplet interfacial tension ($\gamma_{\mathrm{L\_O}}$) according to Tadmor's approach,[30–33] which is represented as:

$$f_{\parallel} = \frac{\gamma_{\mathrm{L\_O}} W(\cos\theta_{\mathrm{R}} - \cos\theta_{\mathrm{A}})\Delta P}{G_{\mathrm{s}}}, \quad (5)$$

where W is the width of the droplet (Fig. 2c), and θ_{R} and θ_{A} are the receding and advancing contact angles, respectively. ΔP is the Laplace pressure difference between the inside and the outside of the droplet near the three-phase contact line. G_{s} is the shear modulus that is associated with the outermost layer of the solid surface. The Furmidge equation[34] is not used here considering that it is not appropriate to describe the onset of droplet motion.[33] The decreased retentive force facilitates the lateral actuation of the organic droplet on the PPy(DBS) electrodes.

The change of the wetting properties of a PPy(DBS) surface as shown in Fig. 2b was complete in ~2 seconds. The switching time of wetting properties relates to the process of the electrochemical reaction of PPy(DBS). Fig. 2d shows the change in the chronoamperometric current during multiple redox cycles. The change in current indicates the charges consumed by the PPy(DBS) film[15] and the occurrence of the electrochemical reaction of the PPy(DBS) coating. The current declined dramatically in the initial ~2 seconds during both reduction and oxidation processes, implying rapid redox kinetics in PPy(DBS) films upon the application of voltages. Subsequently, the change in the current became moderate and eventually reached the background current, indicating that the electrochemical reaction (*i.e.*, reduction or oxidation) of the PPy(DBS) film has been completed.

3.2. Droplet actuation on PPy(DBS) electrodes

Based on the tunable wettability of the PPy(DBS) surfaces, we demonstrated the lateral actuation process of a DCM droplet on an array of two PPy(DBS) electrodes. Fig. 3 shows the fabricated PPy(DBS) electrodes used for the demonstration. The PPy(DBS) electrode patterns are composed of a PPy(DBS) coating and underlying Au/Cr conductive layers on an SiO_2 coated Si substrate (Fig. 3a). Fig. 3b illustrates the configuration of two PPy(DBS) electrodes. Fig. 3c is the cross-sectional view of a PPy(DBS) electrode, showing the coated PPy(DBS) film with the embedded Au/Cr layers. The PPy(DBS) film was 1.3 μm thick as it was electrodeposited at 0.8 V with a surface charge density of 150 mC cm^{-2}.

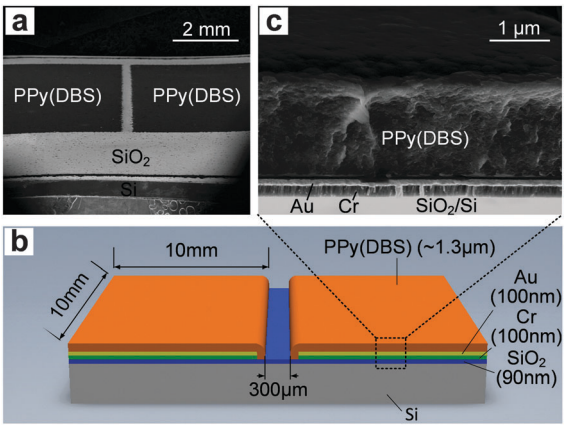

Fig. 3 Schematic and fabrication result of PPy(DBS) electrodes. (a) SEM image (tilting view) of the fabricated PPy(DBS) electrodes. (b) Schematic of the configuration of two PPy(DBS) electrodes (not to scale). (c) Cross-sectional view of the PPy(DBS) electrode.

Fig. 4a depicts the lateral actuation process of a DCM droplet on two PPy(DBS) electrodes. Two PPy(DBS) electrodes were initially oxidized at a voltage of 0.6 V (*vs.* the counter electrode). A DCM droplet (~6 μL) was then placed on the surface of the pair of PPy(DBS) electrodes (Fig. 4a-i). Once the droplet was adequately in contact with both electrodes, a reductive voltage of −0.9 V (*vs.* counter electrode) was applied to activate the PPy(DBS) electrode on the left (Fig. 4a-i). Upon the reduction of the left electrode, the droplet was flattened in ~2 seconds with an increased contact angle (Fig. 4a-ii), similar to the situation shown in Fig. 2. The flattened droplet then gradually moved from the activated (left) electrode to the non-activated (right) one. In ~10 seconds, the droplet was completely transported to the non-activated electrode on the right (Fig. 4a-vi). Fig. 4b illustrates the sequential redox reaction in PPy(DBS) electrodes and the resulting change in interfacial tensions that facilitates droplet actuation. In the initial state, both PPy(DBS) electrodes are in oxidized states (Fig. 4b-i). The interfacial tensions acting on the contact lines of the droplet on two electrodes are equal, and the net lateral interfacial tension force experienced by the droplet is zero. The application of a reductive voltage to the PPy(DBS) electrode on the left in Fig. 4b-ii reduces the PPy(DBS) surface exposed to the electrolyte. A lateral driving force is then generated on the droplet due to the imbalanced interfacial tensions and is directed towards the non-activated electrode on the right, as discussed in eqn (1). Meanwhile, the droplet flattens along with the decrease of interfacial tension, indicating the decrease of the retentive force of the droplet on the surface, as explained in Fig. 2. Under the lateral driving force accompanied by the decrease of the retentive force, the droplet moves from the activated electrode to the non-activated electrode (Fig. 4b-iii). With the movement of the droplet, the PPy(DBS) surface, which is initially underneath the droplet on the activated electrode, is now exposed to the electrolyte and further reduced along with the absorption of cations from the surrounding electrolyte (Fig. 4b-iv). Therefore, the boundary between the reduced and the oxidized PPy(DBS) surfaces on

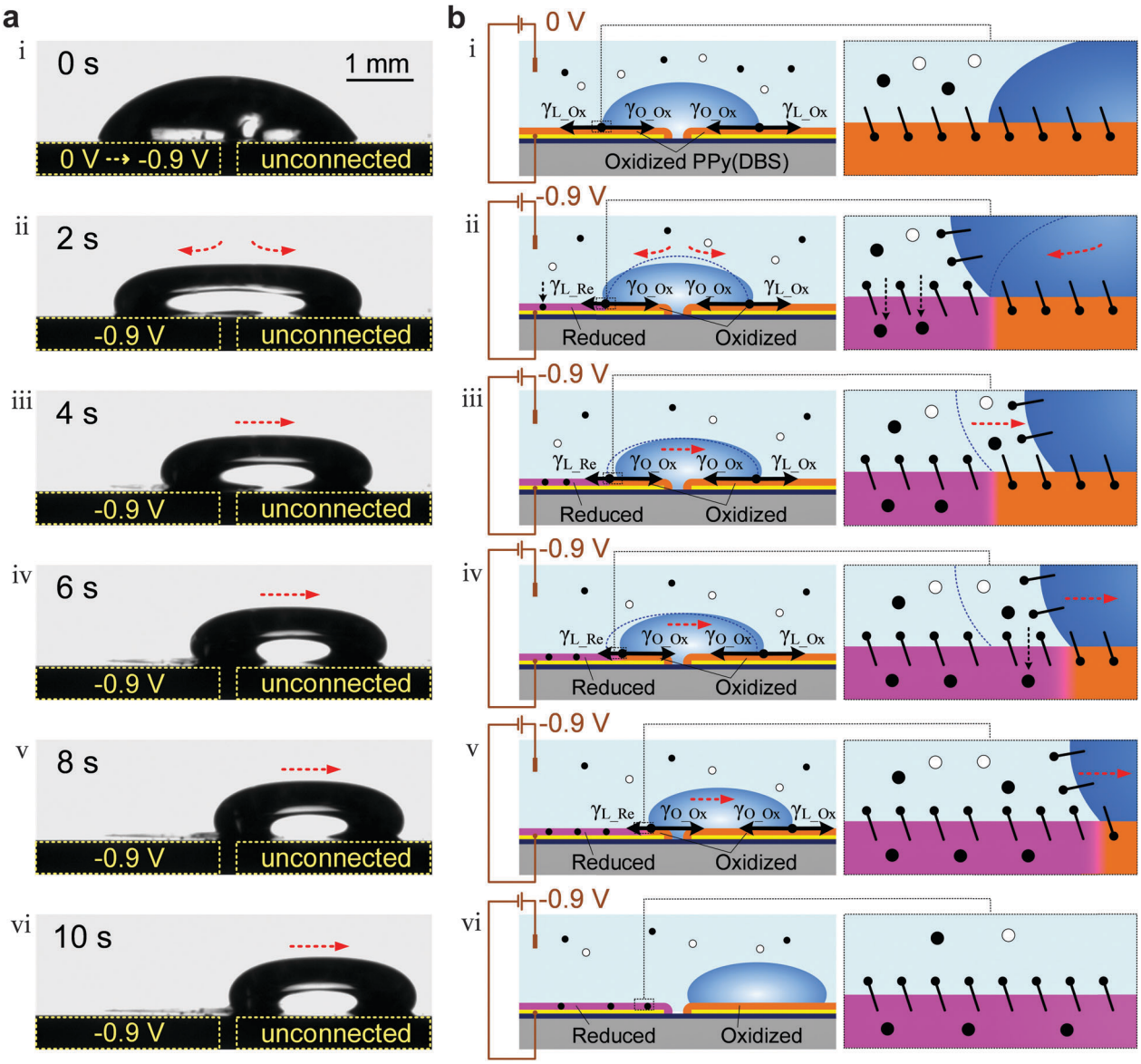

Fig. 4 (a) Lateral actuation process of a DCM droplet in 0.1 M $NaNO_3$ solution. The two PPy(DBS) electrodes (marked as dotted lines) are independently addressable. (b) Schematics of the redox reaction in PPy(DBS) electrodes and the change of lateral interfacial tensions acting on the droplet during the actuation.

the activated electrode moves in accordance with the contact line of the droplet, which provides a sustained driving force for the continuous movement of the droplet (Fig. 4b-v). Once the droplet is completely transported to the adjacent electrode, the PPy(DBS) surface on the activated electrode is totally reduced when fully exposed to the electrolyte (Fig. 4b-vi). The reduced PPy(DBS) electrode is reoxidized for reuse by applying an oxidation voltage of 0.6 V.

The actuation process of a DCM droplet on the PPy(DBS) electrodes, as shown in Fig. 4, exhibits four different states according to the behavior of the droplet motion. The first state (referred to as State I in Fig. 5) corresponds to the reduction process of the PPy(DBS) surface and the flattening of the droplet (*i.e.*, Fig. 4a-i and ii), which lasted for 1–2 seconds. In State II, both rear and front contact lines of the droplet moved toward the electrode on the right (*i.e.*, Fig. 4a-ii and iv). The rear contact line of the droplet receded rapidly, and 75% of the displacement of the rear contact line was completed in this state. In addition, the receding of the rear contact line of the droplet on the activated electrode was more significant than the advancing of the front contact line of the droplet on the non-activated electrode in this state. We attribute this to the pinning effect at the front contact line of the organic droplet on the oxidized (less oleophobic) PPy(DBS) surface, which is stronger than that at the rear contact line of the droplet on the reduced (more oleophobic) PPy(DBS) surface. The difference in the pinning effect results in the different displacements of front and rear contact lines of the droplet, and consequently the change of droplet shape

(*i.e.*, a moderate decrease of the width and an increase of the height as shown in Fig. 4a) during the actuation. The following state (State III) is a deceleration state in the actuation process (*i.e.*, Fig. 4a-iv–vi), compared with State II. The droplet was completely transported to the non-activated electrode after State III and then stops after a slight movement of the contact lines due to an inertial effect. This is the final stabilized state of the actuation process (State IV).

As shown in Fig. 5b, the average receding velocity of the rear contact line of the droplet in State I was $\sim$0.14 mm s^{-1}, and then rapidly increased to $\sim$0.40 mm s^{-1} in State II, followed by a gradual decrease in States III and IV. The advancing velocity of the front contact line of the droplet in States I and II was smaller than the receding velocity of the rear contact line of the droplet, and gradually increased to the maximum value of 0.15 mm s^{-1} until State III, where it decreased at a similar pace with the receding velocity of the rear contact line. The change of velocity of the droplet center was similar to the receding velocity of the rear contact line; it gradually increased to the maximum value of 0.22 mm s^{-1} in State II. The net effective force (*i.e.*, the difference between driving force and resistance forces) experienced by the moving droplet is estimated using the acceleration of the droplet in the acceleration state (*i.e.*, the initial 3 seconds) during the actuation. The net effective force is represented as:

$$F_{net} = ma, \quad (6)$$

where m is the mass of droplet and a is the acceleration. For the droplet in Fig. 4, the mass is $\sim 8 \times 10^{-6}$ kg and acceleration is $\sim$0.07 mm s^{-2}. The estimated net effective force therefore is approximately 10^{-10} N.

Fig. 5c shows the change of contact angles of both the receding and the advancing sides of the DCM droplet during the actuation. The contact angles of the droplet on both activated and non-activated PPy(DBS) electrodes were increased from $\sim 60^\circ$ to $\sim 120^\circ$ in 2 seconds along with the flattening of the droplet in State I. It should be noted that the initial contact angle is smaller than the apparent contact angle of a DCM droplet on the oxidized PPy(DBS) in a stabilized state as shown in Fig. 2. The reason is that the droplet placed across two electrodes was formed by merging two smaller droplets, initially dispensed on each PPy(DBS) electrode (the details are described in the Experimental section), and the pinning effect of the droplet contact line on each oxidized PPy(DBS) electrode caused the decrease in the contact angle of the newly formed droplet during the merging. The contact angles then continuously increased and became stable at $\sim 140^\circ$ during the actuation (*i.e.*, States II and III). The difference between the advancing contact angle and the receding contact angle (*i.e.*, contact angle hysteresis) was smaller than 2° during the actuation, indicating that the movement of the droplet was enabled under a low retentive force. The retentive force is estimated to be approximately 10^{-7} N according to eqn (5) (the shear modulus, G_S, in eqn (5) is estimated by using the Young's modulus (E) of an oxidized PPy(DBS) thin film since the PPy(DBS) surface underneath the droplet is in the oxidized

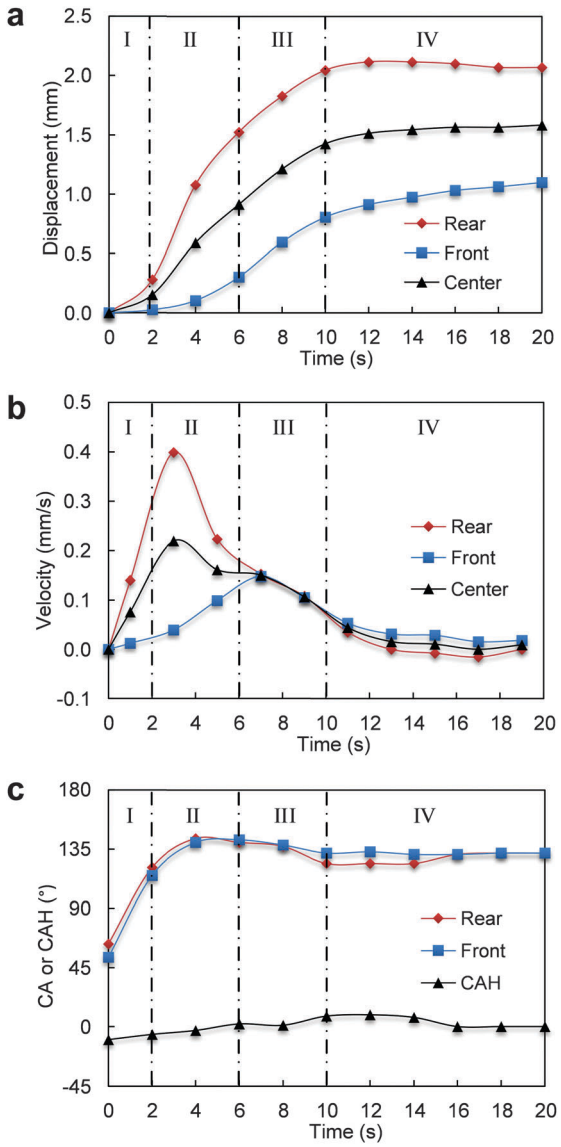

Fig. 5 (a) Displacement and (b) velocity of the rear contact line, the front contact line, and the center of a DCM droplet during the actuation process, respectively. (c) Contact angles (CA) of the rear (receding) side and the front (advancing) side of a DCM droplet and the contact angle hysteresis (CAH, the difference between the CAs of the advancing and receding sides). The droplet actuation process shows four different states: starting (State I), acceleration (State II), deceleration (State III), and stabilization (State IV).

state, which is reported to be between 0.12 and 0.20 GPa,[35] with the Poisson ratio (ν) of 0.4[36] ($G_S = E/2(1+\nu)$); R_{d1} and R_{d2} shown in Fig. 2c are used to estimate the principal radii of curvature of the droplet at the three-phase contact line to calculate ΔP ($\Delta P = \gamma_{L\_O}(1/R_{d1} + 1/R_{d2})$). The moving droplet concurrently experiences a drag force due to the viscosity of the surrounding medium, which is proportional to the velocity of the droplet. According to Stokes law,[37] the drag force is represented as:

$$F_{drag} = 6\pi\mu V R_e, \quad (7)$$

where μ is the viscosity of the liquid, V is the droplet velocity, and R_e is the equivalent radius. The shape of the flattened

droplet shown in Fig. 4 is close to an oblate ellipsoid and R_e equals $(a^2b)^{1/3}$, where a and b are the semi-major axis length and minor axis length, respectively.[38] The estimated drag force is approximately 10^{-9} N, which is two orders of magnitude smaller than the retentive force, indicating that the major resistance for the droplet actuation is the retentive force. The estimated driving force, which is equal to the summation of the retentive force, drag force, and net effective force, is therefore approximately 10^{-7} N.

4. Experimental

4.1. Fabrication of PPy(DBS) electrodes

PPy(DBS) electrodes were fabricated *via* electropolymerization on a silicon dioxide coated silicon substrate, which had been pre-patterned using Au/Cr electrodes. The Au/Cr electrode patterns were deposited on the silicon dioxide surface through a lift-off process. In particular, an oxidized (silicon dioxide: ~90 nm) silicon wafer (WRS Materials, San Jose, CA, USA) was cleaned with acetone, methanol, and de-ionized (DI) water, dried using nitrogen gas, and dehydrated at 110 °C on a hotplate. After hexamethyldisilazane (HMDS) was spin-coated on the wafer as an adhesion promoter, SPR 3012 photoresist (Rohm and Haas Electronic Materials LLC, Marlborough, MA, USA) was spin-coated at 2000 rpm for 1 minute to produce a film with a thickness of ~2 μm. The substrate was then exposed by using a mask aligner (MA-6, SUSS MicroTec, Garching, Germany) in soft-contact mode after soft-baking at 90 °C, and developed by MF-319 (Rohm and Haas Electronic Materials LLC, Marlborough, MA, USA). After the pattern of photoresist was obtained on the substrate, the substrate was coated with Cr (100 nm) and Au (100 nm) using an e-beam evaporator (Explorer 14, Denton Vacuum, Moorestown, NJ, USA). The Cr layer was used to increase the adhesion of the Au layer to the SiO_2 layer. The substrate was then immersed in acetone to remove the underlying photoresist layer, defining the Au/Cr electrode patterns on the silicon dioxide substrate *via* the lift-off process. A two-electrode configuration of Au/Cr electrodes with a gap between the electrodes of approximately 300 μm was fabricated for the demonstration, confirmed using a scanning electron microscope (Auriga small dual-beam FIB-SEM, Carl Zeiss, Jena, Germany). The substrate was then rinsed with methanol and DI water, dried using nitrogen gas, and dehydrated at 110 °C on a hotplate. The PPy(DBS) films were then electropolymerized on the Au/Cr electrodes. During the electropolymerization, the substrate was submerged in a solution consisting of 0.1 M pyrrole (reagent grade, 98%, Sigma-Aldrich, St Louis, MO, USA) and 0.1 M sodium dodecylbenzenesulfonate (NaDBS) (technical grade, Sigma-Aldrich, St Louis, MO, USA) as the working electrode. A saturated calomel electrode (SCE) (Fisher Scientific Inc., Pittsburgh, PA, USA) and an Au-coated silicon wafer were also submerged in the solution as the reference electrode and the counter electrode. The deposition of PPy(DBS) on the Au surface was carried out at 0.8 V *versus* SCE at a setting of 150 mC cm^{-2} surface charge density using a potentiostat (263A, Princeton Applied Research, Oak Ridge, TN, USA).[4] The substrate with the PPy(DBS) electrodes was then cleaned by rinsing with DI water and stored under room conditions. The surface morphologies of the PPy(DBS) coatings were characterized using scanning electron microscopy (Auriga small dual-beam FIB-SEM, Carl Zeiss, Jena, Germany).

In addition to the patterned PPy(DBS) electrodes, PPy(DBS) films coated on unpatterned Au/Cr coated silicon wafers were also prepared using the same parameters to study the tunable wetting of PPy(DBS) surfaces.

4.2. Characterization of the tunable wetting of PPy(DBS) surfaces

The surface wetting properties of the PPy(DBS) films coated on the unpatterned Au/Cr coated silicon wafer were characterized by measuring the contact angles of DCM droplets in 0.1 M $NaNO_3$ (≥99.0%, Sigma-Aldrich, St Louis, MO, USA) solution during oxidation and reduction using a goniometer (Model 500, Ramé-hart, Netcong, NJ). The configuration of the experimental setup is shown in Fig. S1 in the ESI.† The PPy(DBS) samples were oxidized and reduced as the working electrode in a quartz cell (45 mm × 30 mm × 45 mm deep) filled with 0.1 M $NaNO_3$. A copper tape was used as the counter electrode, which was vertically placed in the $NaNO_3$ solution at a corner of the quartz cell. A saturated calomel electrode (SCE) was used as a reference electrode. A voltage of 0.6 V was used for the oxidation. After oxidation, a DCM droplet was placed on the PPy(DBS) electrodes in 0.1 M $NaNO_3$, and the contact angles were measured using the goniometer. A voltage of −0.9 V was then applied to the PPy(DBS) surface for the reduction. The changes of the contact angles of the droplet were recorded. The tunable wetting properties of the PPy(DBS) surface during multiple redox cycles were studied by switching the voltage between 0.6 V and −0.9 V. In each redox cycle, a new DCM droplet was used for the contact angle measurements. The voltages of oxidation/reduction were chosen according to the cyclic voltammogram of the reduction–oxidation reaction of PPy(DBS).[4] We also studied the change of the electric current during oxidation and reduction of the PPy(DBS) to analyze the electrochemical reaction of PPy(DBS). The interfacial tension of a DCM droplet in 0.1 M $NaNO_3$ solution was also measured by the pendant droplet method using the goniometer.

4.3. Actuation of organic droplets on PPy(DBS) electrodes

The lateral actuation of DCM droplets on two PPy(DBS) electrodes was demonstrated in 0.1 M $NaNO_3$ using the potentiostat in a two-electrode configuration (*i.e.*, working and counter electrodes). Two PPy(DBS) electrodes were initially oxidized at 0.6 V, using the potentiostat with copper tape as the counter electrode. A DCM droplet was then placed on the top of the pair of two PPy(DBS) electrodes. Since the DCM droplet tended to remain on only one of the PPy(DBS) electrodes when placed between two PPy(DBS) electrodes due to the repelling effect of the oleophobic dielectric gap (SiO_2 layer), two small droplets were first placed on each electrode, where they were merged by adding a small extra volume between them to form a single

droplet across two PPy(DBS) electrodes. The formed single droplet shows a smaller contact angle than the initial small droplets due to the significant pinning of the droplet contact line on each electrode during the combination. After the DCM droplet was placed, a voltage of −0.9 V was applied to a PPy(DBS) electrode and copper tape was used as the counter electrode. No voltage was applied to the other PPy(DBS) electrode. The actuation process was recorded using the camera of the goniometer.

5. Conclusions

We have demonstrated the controlled lateral actuation of a DCM droplet on PPy(DBS) electrodes in an aqueous environment. The tunable wetting of PPy(DBS) surfaces during redox reactions created imbalanced interfacial tensions on the droplet placed across the reduced and oxidized PPy(DBS) electrodes. The imbalanced interfacial tensions facilitated the translation of the droplet from the reduced electrode to the oxidized electrode at ∼0.9 V. The droplet actuation between two electrodes initiated at ∼2 seconds upon the application of the voltage and completed in ∼10 seconds. The driving force for the droplet actuation was approximately 10^{-7} N for a 6 μL droplet. This demonstration and elucidation of the mechanism of droplet's lateral actuation warrants further study towards the development of low-voltage microfluidic devices for cross-disciplinary applications.

Acknowledgements

This work has been supported in part by a National Science Foundation award (ECCS-1202269). This work has also been partially carried out at the Micro Device Laboratory funded by support from Contract# W15QKN-05-D-0011, and Laboratories for Multiscale Imaging (LMSI) at Stevens Institute of Technology. The authors also thank Anthony Palumbo for his valuable comments.

References

1 G. G. Wallace, P. R. Teasdale, G. M. Spinks and L. A. P. Kane-Maguire, *Conductive electroactive polymers: intelligent polymer systems*, CRC Press, 2008.
2 E. Smela, *J. Micromech. Microeng.*, 1999, **9**, 1–18.
3 K. S. Teh, Y. Takahashi, Z. Yao and Y.-W. Lu, *Sens. Actuators, A*, 2009, **155**, 113–119.
4 Y.-T. Tsai, C.-H. Choi, N. Gao and E. H. Yang, *Langmuir*, 2011, **27**, 4249–4256.
5 J. H. Chang and I. W. Hunter, *Macromol. Rapid Commun.*, 2011, **32**, 718–723.
6 J. Isaksson, C. Tengstedt, M. Fahlman, N. D. Robinson and M. Berggren, *Adv. Mater.*, 2004, **16**, 316–320.
7 J. P. Giesy, J. E. Naile, J. S. Khim, P. D. Jones and J. L. Newsted, in *Reviews of Environmental Contamination and Toxicology*, ed. D. M. Whitacre, Springer, New York, 2010, pp. 1–52.
8 J. Causley, S. Stitzel, S. Brady, D. Diamond and G. Wallace, *Synth. Met.*, 2005, **151**, 60–64.
9 G. Chatzipirpiridis, A. Sanoria, O. Ergeneman, J. Sort, J. Puigmartí-Luis, B. J. Nelson, E. Pellicer and S. Pané, *Electrochem. Commun.*, 2015, **54**, 32–35.
10 Y.-T. Tsai, C.-H. Choi and E. H. Yang, *Lab Chip*, 2012, **13**, 302–309.
11 W. Xu, J. Xu, C.-H. Choi and E. H. Yang, *ACS Appl. Mater. Interfaces*, 2015, **7**, 25608–25617.
12 I. F. Uchegbu and A. G. Schatzlein, *Polymers in drug delivery*, CRC Press, 2006.
13 B. Su, S. Wang, Y. Song and L. Jiang, *Soft Matter*, 2011, **7**, 5144–5149.
14 C. Ding, Y. Zhu, M. Liu, L. Feng, M. Wan and L. Jiang, *Soft Matter*, 2012, **8**, 9064–9068.
15 X. Wang and E. Smela, *J. Phys. Chem. C*, 2009, **113**, 359–368.
16 X. Wang and E. Smela, *J. Phys. Chem. C*, 2009, **113**, 369–381.
17 X. Wang, B. Shapiro and E. Smela, *Adv. Mater.*, 2004, **16**, 1605–1609.
18 J. Berthier, *Micro-drops and digital microfluidics*, William Andrew, 2012.
19 M. Liu, F.-Q. Nie, Z. Wei, Y. Song and L. Jiang, *Langmuir*, 2010, **26**, 3993–3997.
20 L. Bay, T. Jacobsen, S. Skaarup and K. West, *J. Phys. Chem. B*, 2001, **105**, 8492–8497.
21 P. R. Waghmare, S. Das and S. K. Mitra, *Sci. Rep.*, 2013, **3**, 1862.
22 Y. Takahashi, K. S. Teh and Y. W. Lu, in *The 22nd IEEE International Conference on Micro Electro Mechanical Systems (MEMS 2009)*, Sorrento, 2009, pp. 459–462.
23 Q. Pei and O. Inganäs, *J. Phys. Chem.*, 1993, **97**, 6034–6041.
24 T. Matencio, M.-A. De Paoli, R. C. D. Peres, R. M. Torresi and S. I. Córdoba de Torresi, *J. Braz. Chem. Soc.*, 1994, **5**, 191–196.
25 T. Matencio, M.-A. De Paoli, R. C. D. Peres, R. M. Torresi and S. I. Córdoba de Torresi, *Synth. Met.*, 1995, **72**, 59–64.
26 C. E. Stauffer, *J. Phys. Chem.*, 1965, **69**, 1933–1938.
27 R. J. Roe, V. L. Bacchetta and P. M. G. Wong, *J. Phys. Chem.*, 1967, **71**, 4190–4193.
28 M. E. R. Shanahan, *J. Phys. D: Appl. Phys.*, 1987, **20**, 945–950.
29 A. Carré, J.-C. Gastel and M. E. R. Shanahan, *Nature*, 1996, **379**, 432–434.
30 R. Tadmor, P. Bahadur, A. Leh, H. E. N'Guessan, R. Jaini and L. Dang, *Phys. Rev. Lett.*, 2009, **103**, 266101.
31 R. Tadmor, *Langmuir*, 2013, **29**, 15474–15475.
32 A. Leh, H. E. N'guessan, J. Fan, P. Bahadur, R. Tadmor and Y. Zhao, *Langmuir*, 2012, **28**, 5795–5801.
33 R. Tadmor, *Soft Matter*, 2011, **7**, 1577–1580.
34 C. G. Furmidge, *J. Colloid Sci.*, 1962, **17**, 309–324.
35 M. Christophersen, B. Shapiro and E. Smela, *Sens. Actuators, B*, 2006, **115**, 596–609.
36 V. Ho, A. G. Narenji, L. Kulinsky and M. Madou, *J. Micro-electromech. Syst.*, 2015, **24**, 1616–1621.
37 R. W. Fox, P. J. Pritchard and A. T. McDonald, *Introduction to fluid mechanics*, Wiley, 7th edn, 2008.
38 V. A. Bloomfield, *On-Line Biophysics Textbook: Separations and Hydrodynamics*, 2000.